Structure, Ferromagnetic Ordering, Anisotropy, and Spin Reorientation for the Two-Dimensional Cyano-Bridged Bimetallic Compound $K_2Mn_3(H_2O)_6[Mo(CN)_7]_2 \cdot 6H_2O$

Joulia Larionova,[†] Olivier Kahn,*[,†] Stéphane Gohlen,[‡] Lahcène Ouahab,[‡] and Rodolphe Clérac[†,§]

Contribution from the Laboratoire des Sciences Moléculaires, Institut de Chimie de la Matière Condensée de Bordeaux, UPR CNRS No. 9048, 33608 Pessac, France, Laboratoire de Chimie du Solide et Inorganique Moléculaire, UMR CNRS No. 6511, Université de Rennes 1, 35042 Rennes, France, and Centre de Recherche Paul Pascal, UPR CNRS No. 8641, 33600 Pessac, France

Received September 14, 1998

Abstract: The title compound, $K_2Mn_3(H_2O)_6[Mo(CN)_7]_2 \cdot 6H_2O$, has been synthesized by slow diffusion of aqueous solutions saturated in KNO_3 and containing $K_4[Mo(CN)_7] \cdot 2H_2O$ and $[Mn(H_2O)_6](NO_3)_2$, respectively. The compound crystallizes in the monoclinic system, space group *C*2. The Mo site is surrounded by six −C−N−Mn linkages and one terminal cyano group in a strongly distorted pentagonal bipyramid fashion. There are two distorted octahedral Mn sites, both with four −N−C−Mo linkages and two water molecules in trans conformation. The structure is two-dimensional with anionic layers perpendicular to the *a* axis and K^+ ions located between the layers. Each layer is constituted of two parallel gridlike sheets made of edge-sharing Mo_2Mn_2 lozenge motifs, connected by $Mn(CN)_4(H_2O)_2$ units situated between the sheets. Thorough magnetic investigations have been carried out. First, it has been demonstrated that the magnetic axes are collinear with the *a*, *b*, and *c** crystallographic directions. The temperature and field dependences of the magnetization in both the dc and ac modes have been measured along the principal axes. The angular dependence of the magnetization in the *bc** plane as a function of the external field has also been measured. These investigations have revealed that the compound orders ferromagnetically at $T_c = 39$ K, with a small hysteresis effect along the *c** axis. Furthermore, a field-induced spin reorientation has been detected. The *b* axis is the easy magnetization axis in low field, and the *bc** plane is very anisotropic. When the field reaches a critical value, the *bc** plane becomes almost isotropic. From the magnetic data, the magnetic phase diagram has been determined. When a single crystal of $K_2Mn_3(H_2O)_6[Mo(CN)_7]_2 \cdot 6H_2O$ is partially dehydrated under vacuum, its shape remains unchanged, but T_c is shifted up to 72 K, and the spin reorientation is suppressed. The partially dehydrated material presents a coercive field of 1.3 kOe along *b* at 5 K. These findings have been compared to those reported recently for a three-dimensional material of the same family (the α-phase $Mn_2(H_2O)_5Mo(CN)_7 \cdot 4H_2O$).

Introduction

The studies concerning the Prussian-blue phases in the past few years have provided important insights on the magnetism of polymetallic compounds obtained from molecular precursors.[1−18] The rational design of high-temperature magnets, using the theoretical models developed in molecular magnetism, is one of the remarkable results of these studies.[11−17] In this respect, the high symmetry of the Prussian-blue phases was a favorable situation to fine-tune the magnetic properties of these compounds and obtain a material ordering above room temperature.[19,20] As a matter of fact, the nature of the interaction

* Corresponding author.
[†] Institut de Chimie de la Matière Condensée de Bordeaux.
[‡] Université de Rennes 1.
[§] Centre de Recherche Paul Pascal.

(1) Bozorth, R. M.; Williams, H. J.; Walsh, D. E. *Phys. Rev.* **1956**, *103*, 572.
(2) Holden, A. N.; Matthias, B. T.; Anderson, P. W.; Lewis, H. W. *Phys. Rev.* **1956**, *102*, 1463.
(3) Herren, F.; Fischer, P.; Ludi, A.; Hälg, W. *Inorg. Chem.* **1980**, *19*, 956.
(4) Ludi, A.; Güdel, H. U. *Struct. Bonding (Berlin)* **1973**, *14*, 1.
(5) Klenze, R.; Kanellakopoulos, B.; Trageser, G.; Eysel, H. *J. Chem. Phys.* **1980**, *72*, 5819.
(6) Griebler, W. D.; Babel, D. *Z. Naturforsch. B* **1982**, *37*, 832.
(7) Babel, D. *Comments Inorg. Chem.* **1986**, *5*, 285.
(8) Babel, D.; Kurtz, W. In *Solid State Chemistry 1982*; Metselaar, R., Heijligers, H. J. M., Schoonman, J., Eds.; Elsevier: Amsterdam, 1983.
(9) Kurtz, W.; Babel, D. *Solid State Commun.* **1983**, *48*, 277.
(10) Gadet, V.; Bujoli-Doeuff, M.; Force, L.; Verdaguer, M.; Malkhi, K. E.; Deroy, A.; Besse, J. P.; Chappert, C.; Veillet, P.; Renard, J. P.; Beauvillain, P. In *Magnetic Molecular Materials*; Gatteschi, D., Kahn, O., Miller, J. S., Palacio, F., Eds.; NATO ASI Series E 198; Plenum: New York, 1991.
(11) Gadet, V.; Mallah, T.; Castro, I.; Verdaguer, M. *J. Am. Chem. Soc.* **1992**, *114*, 9213.
(12) Mallah, T.; Thiébaut, S.; Verdaguer, M.; Veillet, P. *Science* **1993**, *262*, 1554.
(13) Mallah, T.; Ferlay, S.; Auberger, C.; Helary, C.; L'Hermite, F.; Ouahès, R.; Vassermann, J.; Verdaguer, M.; Veillet, P. *Mol. Cryst. Liq. Cryst.* **1994**, *273*, 141.
(14) Ferlay, S.; Mallah, T.; Ouahès, R.; Veillet, P.; Verdaguer, M. *Nature* **1995**, *378*, 701.
(15) Entley, W. R.; Treadway, C. R.; Girolami, G. S. *Mol. Cryst. Liq. Cryst.* **1994**, *273*, 153.
(16) Entley, W. R.; Girolami, G. S. *Science* **1995**, *268*, 397.
(17) Entley, W. R.; Girolami, G. S. *Inorg. Chem.* **1994**, *33*, 5165.
(18) Sato, O.; Iyoda, T.; Fujishima, A.; Hashimoto, K.; *Science* **1996**, *272*, 704.
(19) Kahn, O. *Adv. Inorg. Chem.* **1995**, *43*, 179.

10.1021/ja9832717 CCC: $18.00
Published on Web 03/23/1999

betweentwo nearest neighbor 3d magnetic ions is governed by symmetry rules involving the singly occupied orbitals.[21] When the symmetry of the magnetic sites is lowered, the applicability of these rules tends to vanish. In particular, the situation of strict orthogonality of the magnetic orbitals leading to ferromagnetic interactions disappears. The presence of 4d and 5d magnetic ions also makes these symmetry rules less heuristic as a result of the strong orbital mixing through spin−orbit coupling.[22] To some extent, it is possible to say that high symmetry, 3d spin carriers, and predictable magnetic properties constitute a consistent set.[23] Conversely, low symmetry, 4d spin carriers, and novel and unpredictable physical properties might constitute another consistent set. The work concerning the cyano-bridged bimetallic species synthesized from the $[Mo^{III}(CN)_7]^{4-}$ precursor, initiated a year ago,[24,25] is inspired by this idea. Let us point out that the Mo^{III} ion in the $[Mo(CN)_7]^{4-}$ chromophore is low-spin, with a $S_{Mo} = {}^1/_2$ local spin,[26] and that the **g**-tensor associated with the ground Kramers doublet is very anisotropic.[27]

Recently, we reported on two phases of formula $Mn_2(H_2O)_5Mo(CN)_7 \cdot nH_2O$ (α-phase, $n = 4$; β-phase $n = 4.75$),[24] then described the magnetic properties of the α-phase in great detail.[25] Single-crystal magnetic measurements allowed us to determine the magnetic phase diagram of this compound. This paper is devoted to a novel compound of the family, of formula $K_2Mn_3(H_2O)_6[Mo(CN)_7]_2 \cdot 6H_2O$. We will first describe the two-dimensional crystal structure, and then focus on the single-crystal magnetic properties. Both dc and ac magnetic measurements will be reported, and the magnetic phase diagram of the compound will be established. We will also study the effect of partial dehydration on the magnetic properties. Finally, we will analyze our findings.

Experimental Section

Synthesis. $K_4[Mo(CN)_7] \cdot 2H_2O$ was prepared as already described.[26−28] Well-shaped and rather large (up to $1.5 \times 1.5 \times 0.5$ mm^3) single crystals of the title compound were obtained by slow diffusion, in an H-shaped tube under nitrogen, of two deoxygenated aqueous solutions almost saturated in KNO_3 and containing $K_4[Mo(CN)_7] \cdot 2H_2O$ and $[Mn(H_2O)_6](NO_3)_2$, respectively, at the concentrations of 10^{-4} M. The crystals have the shape of irregular hexagonal prisms. The *a* axis corresponds to the axis of the prism, and the *bc* plane corresponds to the face of the prism, as shown in Figure 4.

Crystallographic Data Collection and Structure Determination. The crystals are air-sensitive and often consist of agglomerates of thin sheets, which is a consequence of the two-dimensional character of the structure. The refinement of this structure proved to be difficult. A small crystal was embedded in oil and mounted on an Enraf-Nonius CAD4 diffractometer with use of Mo Kα radiation. The data collection was performed at room temperature. After a semiempirical ψ-scan[29] absorption correction, the data reduction was performed using MolEN[30] while structure solution and refinement were carried out using the programs SHELXS-86 and SHELXL-93.[31] Only the Mo, Mn, and K atoms were refined anisotropically. Selected crystal data are given in Table 1.

Table 1. Selected Crystal Data for $K_2Mn_3(H_2O)_6[Mo(CN)_7]_2 \cdot 6H_2O$

formula	$C_{14}H_{24}N_7O_{12}K_2Mn_3Mo_2$
formula weight	1015.4
space group	*C*2
a, Å	31.019(12)
b, Å	7.1857(12)
c, Å	8.103(3)
β, deg	96.038(17)
V, Å^3	1796.1(9)
Z	4
diffractometer	Enraf-Nonius
ρ_{calcd}, g cm^{-3}	1.877
no. of data	2257
no. of unique data	2107
no. of parameters	287
μ(Mo Kα), cm^{-1}	0.710 73 Å
R1[a]	0.0573
wR2[b]	0.1218

[a] $R1 = \sum||F_o| - |F_c||/\sum|F_o|$. [b] $wR2 = \{\sum[w(F_o^2 - F_c^2)^2]/\sum[w(F_o^2)^2]\}^{1/2}$.

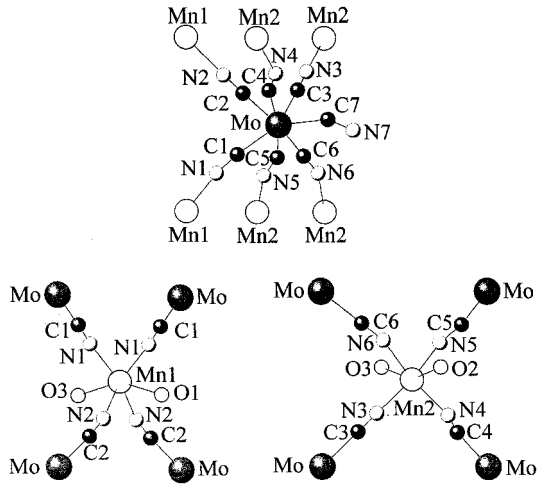

Figure 1. Local structure of the molybdenum and manganese sites.

Magnetic Measurements. These were carried out with a Quantum Design MPMS-5S SQUID magnetometer working down to 2 K and up to 50 kOe. This apparatus was equipped with a horizontal goniometer. The compound is air-sensitive, and all the magnetic investigations were carried out with either single crystals protected with oil or polycrystalline samples placed in a quartz tube and sealed under vacuum.

Description of the Structure

The structure contains a unique Mo site along with two Mn sites, denoted as Mn1 and Mn2, as shown in Figure 1. The molybdenum atom is surrounded by two −C−N−Mn1 linkages, four −C−N−Mn2 linkages, and a terminal −C−N ligand. In other terms, six cyano ligands are bridging, and one is terminal. The symmetry of the Mo site is very low. However, the geometry around Mo may be viewed as a strongly distorted pentagonal bipyramid with Mo−C4−N4 and Mo−C6−N6 along the axial directions, and a C4−Mo−C6 angle of 161.3(8)°, instead of 180° for a regular pentagonal bipyramid. The C−Mo−C bond angles within the equatorial plane range from 65.7(8) to 79.2(7)°, their sum being equal to 374.0°. These

(20) Kahn, O. *Nature* **1995**, *378*, 667.
(21) Kahn, O. *Molecular Magnetism*; VCH: New York, 1993.
(22) Larionova, J.; Mombelli, B.; Sanchiz, J. Kahn, O. *Inorg. Chem.* **1998**, *37*, 679.
(23) Kahn, O. *Angew. Chem., Int. Ed. Engl.* **1985**, *24*, 834.
(24) Larionova, J.; Sanchiz, J.; Gohlen, S.; Ouahab, L.; Kahn, O. *J. Chem. Soc., Chem. Commun.* **1998**, 953.
(25) Larionova, J.; Clérac, R.; Sanchiz, J.; Kahn, O.; Gohlen, S.; Ouahab, L. *J. Am. Chem. Soc.* **1998**, *120*, 13088.
(26) Rossman, G. R.; Tsay, F. D.; Gray, H. B. *Inorg. Chem.* **1973**, *12*, 824.
(27) Hursthouse, M. B.; Maijk, K. M. A.; Soares, A. M.; Gibson, J. F.; Griffith, W. P. *Inorg. Chim. Acta* **1980**, *45*, L81.
(28) Young, R. C. *J. Am. Chem. Soc.* **1932**, *54*, 1402.
(29) North, A. C. T.; Philips, D. C.; Mathews, F. S. *Acta Crystallogr., Sect. A* **1968**, *A24*, 351.
(30) *MolEN* (Molecular Structure Enraf-Nonius), Enraf-Nonius: Delft, The Netherlands, 1990.
(31) (a) Sheldrick, G. M. *SHELXS-86: Program for the Solution of Crystal Structure*; University of Göttingen: Germany, 1986. (b) Sheldrick, G. M. *SHELXL-93: Program for the Refinement of Crystal Structure*; University of Göttingen: Germany, 1993.

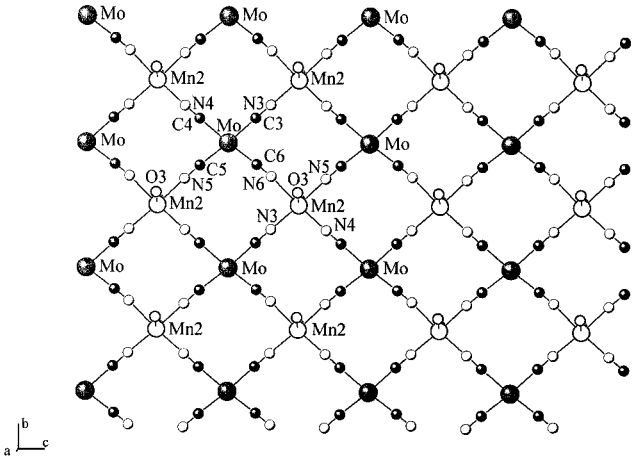

Figure 2. Structure of a gridlike sheet in the *bc* plane.

values are 72 and 360°, respectively, for a D_{5h} geometry. The Mn1 atom is located on a 2-fold rotation axis. It is surrounded by four −N−C−Mo linkages along with two water molecules in *trans* conformation. The geometry around Mn1 may be described as a distorted octahedron. The Mn−N bond lengths are 2.165(16) and 2.209(18) Å, and the Mn−O bond length is 2.279(13) Å. The bond angles range from 70.8(5) to 110.4(5)° and from 151.4(8) to 160.7(5)°, instead of 90 and 180°, respectively, for a perfect octahedron. Mn2 occupies a general position. It is also surrounded by four −N−C−Mo linkages and two water molecules in *trans* conformation. The geometry around Mn2 may also be described as a distorted octahedron. The Mn−N bond lengths range from 2.179(16) to 2.265(17) Å, and the Mn−O bonds are equal to 2.261(11) and 2.341(11) Å. The bond angles range from 72.9(5) to 105.3(5)°, and from 154.3(6) to 167.8(6)°, instead of 90 and 180° for a perfect octahedron.

A striking aspect of the structure lies in the fact that the Mo−C−N−Mn linkages are far from being linear. Both the Mo−C−N and Mn−N−C bond angles significantly deviate from 180°. The former range from 152.2(16) to 176.3(18)° (the mean value is 165.8°). The largest distortion with regard to the linearity involves the terminal cyano group, C7N7. The Mn−

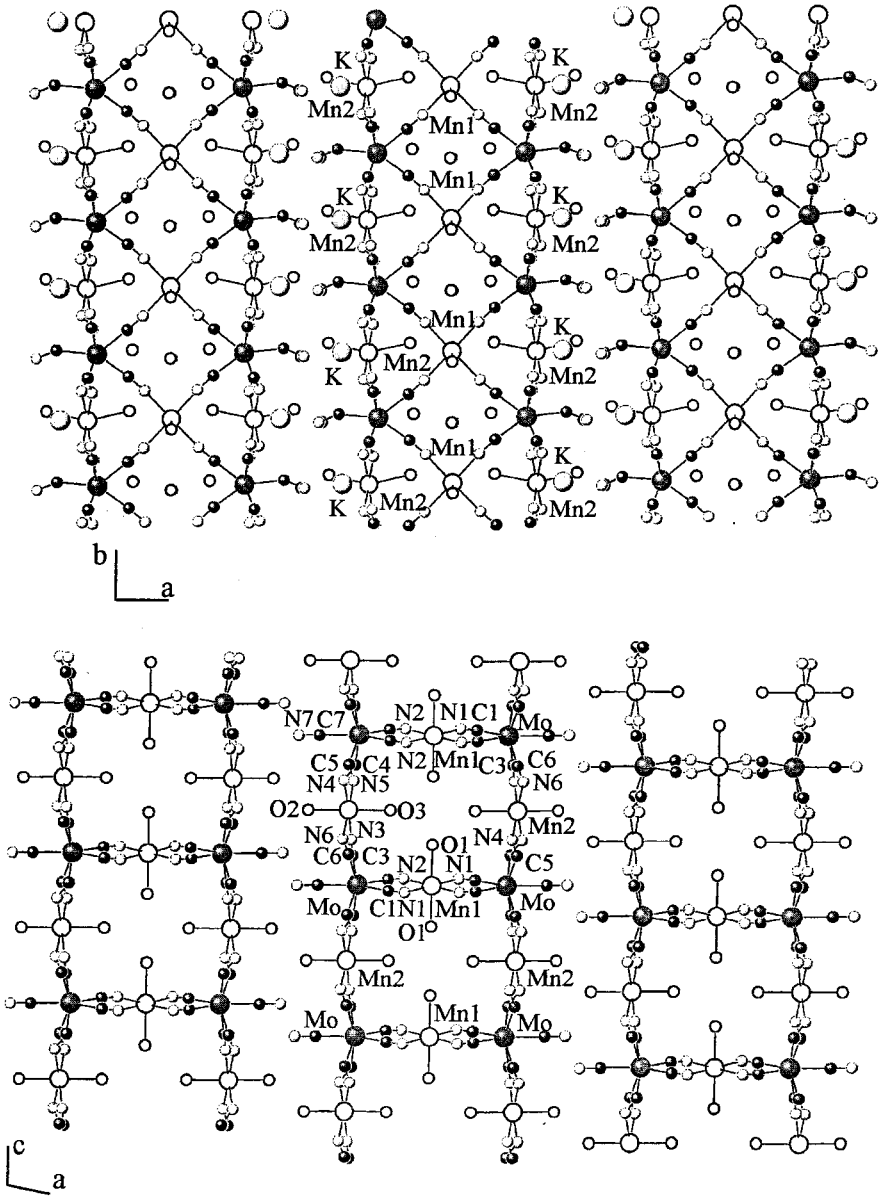

Figure 3. Structure of the compound in the *ab* (top) and *ac* (bottom) planes

N−C bond angles range from 143.8(14) to 179.3(15)° (the mean value is 161.7°).

The structure has a two-dimensional character with anionic double-sheet layers parallel to the *bc* plane, and K^+ and noncoordinated water molecules situated between the layers. Let us first describe a layer. Each sheet is a kind of grid in the *bc* plane made of edge-sharing lozenges [MoC3N3Mn2N4C4-MoC5N5Mn2N6C6], as shown in Figure 2. The Mo−Mn2 separations though a cyano bridge range from 5.433(6) to 5.451(6) Å. The shortest Mo−Mo and Mn2−Mn2 separations corresponding to the diagonals of the lozenges are equal to 8.103(6) and 7.186(8) Å, respectively. Two parallel sheets of a layer are connected by $Mn1(CN)_4(H_2O)_2$ units situated between the sheets, as shown in Figure 3 (*ab* plane). Each $Mn1(CN)_4(H_2O)_2$ unit is linked through cyano bridges to four Mo atoms, two belonging to one of the sheets and two belonging to the other sheet. The Mn1 atoms, together with the Mo atoms to which they are linked, form chains made of corner-sharing lozenges, [MoC1N1Mn1N1C1MoC2N2Mn1N2C2], running along the *b* direction. Within those chains, the Mo−Mn1 separations through a cyano bridge are equal to 5.371(8) and 5.414(8) Å, and the shortest Mo−Mo and Mn1−Mn1 separations are equal to 8.042(4) and 7.186(2) Å, respectively. This Mo−Mo distance of 8.042(6) Å may be considered as the thickness of a layer. Some noncoordinated water molecules are located between the two external sheets of a layer. The thickness of the gap between two layers may be characterized by the shortest metal−metal interlayer separation, namely Mo−Mn2 = 7.263(4) Å (see Figure 3, *ac* plane). Let us note that this shortest separation involves two different metal ions. The shortest Mo−Mo and Mn2−Mn2 interlayer separations are equal to 8.367(3) and 7.436(4) Å, respectively.

The K^+ ions are located between the layers. The closest atom to a K^+ ion is N7 belonging to the nonbridging cyano group, with a K−N7 separation of 2.766(13) Å and a C7−N7−K angle of 131.5(11)°. The second shortest separation is K−O(1W) equal to 2.883(11) Å. K^+ is surrounded by nine other nitrogen and carbon atoms with separations ranging from 3.031(17) to 3.38(2) Å.

Magnetic Properties

We will first determine the magnetic axes, and then we will successively study the temperature and field dependences of the magnetization along the magnetic axes in both the dc and ac modes. We will also characterize a field-induced spin reorientation by measuring the angular dependence of the magnetization in the *bc** plane under different fields.

Determination of the Magnetic Axes. The 2-fold axis of the monoclinic lattice, *b*, is necessarily a magnetic axis. The other two magnetic axes may be determined from the extremes of the magnetization in the *ac* plane. These extremes were found to be along the *a* and *c** directions, as shown in Figure 4 (top). Therefore, the magnetic axes are confounded with the crystallographic axes *a*, *b*, and *c**. The angular dependence of the magnetization was also measured in the *ac** and *bc** planes. The results in the *bc** plane are shown in Figure 4 (bottom). The magnetization is maximum along *b* and minimum along *c**. When the field is increased in the *bc** plane, the rotation figure is dramatically modified. This phenomenon will be investigated in detail below. The rotation figures of Figure 4 reveal that the *b* axis is the easy magnetization axis.

Temperature Dependences of the dc Magnetic Susceptibility and Magnetization. The nature of the dominating interactions was deduced from the $\chi_M T$ versus *T* curve for a polycrystalline sample, shown in Figure 5, χ_M being the magnetic susceptibility per molecular unit and *T* the temperature. $\chi_M T$ is equal to 13.9 emu K mol^{-1} at room temperature, increases more and more rapidly as *T* is lowered, reaches a maximum value around 40 K, then decreases. The room-

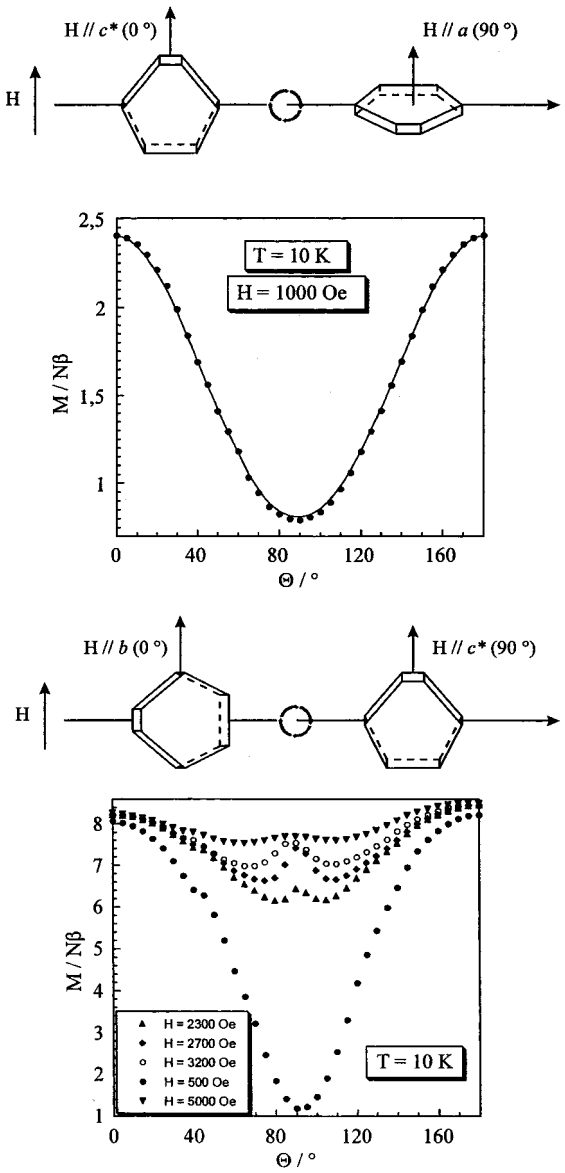

Figure 4. Angular dependences of the magnetization at 10 K: (top) under 1000 Oe in the *acb* plane; (bottom) under different fields in the *bc** plane.

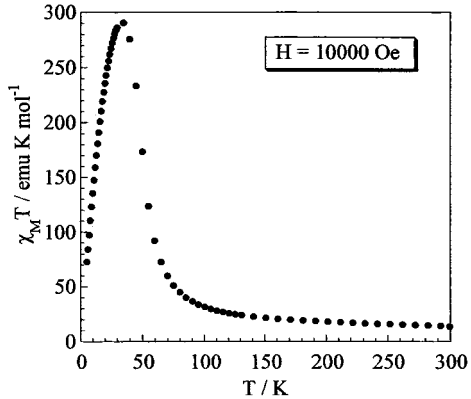

Figure 5. Temperature dependence of $\chi_M T$ for a polycrystalline sample.

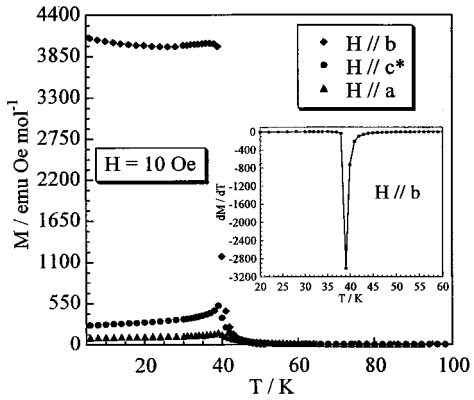

Figure 6. Temperature dependences of the magnetization along the *a*, *b*, and *c** axes under a field of 10 Oe.

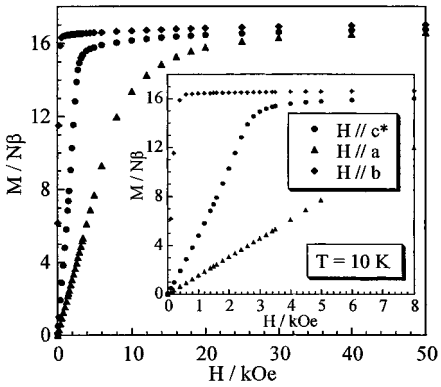

Figure 7. Field dependences of the magnetization at 10 K along the *a*, *b*, and *c** axes.

temperature value of $\chi_M T$ corresponds to what is expected for three Mn^{II} and two Mo^{III} ions, with the local spins $S_{Mn} = {}^5/_2$ and $S_{Mo} = {}^1/_2$. The profile of the curve reveals dominating ferromagnetic interactions.

Figure 6 represents the temperature dependences of the magnetization along the principal axes under a magnetic field of 10 Oe. Along the three directions, *a*, *b*, and *c**, the magnetization shows a break around 39 K. The critical temperature, $T_c = 39$ K, may be determined accurately as the extreme of the derivative d*M*/d*T* (see the insert of Figure 6). The magnetic anisotropy of the compound is very strong. The magnetization is 10 times as large along the easy magnetization axis, *b*, as it is along the other two directions.

Field Dependences of the dc Magnetization. Figure 7 displays the field dependences of the magnetization at 10 K along the three principal directions. Along *b*, the zero field magnetization is very high, which confirms that *b* is the easy magnetization axis, and the saturation is reached under 500 Oe. The saturation magnetization, M_{sat}, is equal to 17 Nβ, which exactly corresponds to the value expected for three $S_{Mn} = {}^5/_2$ and two $S_{Mo} = {}^1/_2$ spins aligned along the field direction. Along *a*, the magnetization increases progressively as the field increases, and it reaches the saturation value above 50 kOe. The *a* axis is the hard magnetization axis. Along *c**, the differential susceptibility, d*M*/d*H*, first increases as *H* increases, changes of sign under 2.4 kOe (inflection point on the $M = f(H)$ curve), then reaches the saturation value. This behavior is characteristic of a field-induced spin reorientation.[32−40] When the field applied along *c** is weak (<2.4 kOe), the spins remain essentially aligned along the easy magnetization axis, *b*. When the field reaches the critical value, $H_c = 2.4$ Oe at 10 K, the spins rotate from the *b* to the *c** axis. Finally, for a field of 3.0 K, called the saturation field, H_{sat}, the spins align along the *c** axis.

To obtain more information on this spin reorientation phenomenon, the angular dependences of the magnetization were measured in the *bc** plane at 10 K for different values of the field (see Figure 4). When the field is sufficiently low, for instance 500 Oe in Figure 4, the maximum is observed along *b* and the minimum along *c**, as already mentioned. When the field increases (see the field values between 2.3 and 3.2 kOe in Figure 4), a secondary maximum of the magnetization is observed along c*, which increases as the field increases, and the magnetic anisotropy in the *bc** plane decreases dramatically. When the value of the saturation field is reached, i.e., 3.0 kOe, the magnetization along *c** is the same as along *b*. The *bc** plane is almost isotropic.

To establish the magnetic phase diagram, it is necessary to determine the temperature dependences of both the critical field, H_c, and the saturation field, H_{sat}.[41] For that, the field dependence of the magnetization along the *c** axis was measured every 5 K in the 5−40 K temperature range. The results are represented in Figure 8 (top). The critical field at each temperature was determined as the field for which the d*M*/d*H* derivative is maximum. The saturation field at each temperature was determined as the weakest field for which the $M = f(H)$ curve is linear. For instance, the saturation field at 10 K is taken as 3.0 kOe. The temperature dependences of H_c and H_{sat} for a field applied along the *c** axis are represented in Figure 8 (bottom). This figure may be viewed as the magnetic phase diagram of the compound. We will come back to this in the discussion section.

The field dependence of the magnetization along *c** at 5 K shows a narrow hysteresis loop with a coercive field of 125 Oe. On the other hand, along the other two directions, no hysteresis is observed. We are faced with a very clean case where the hysteresis observed along *c** arises from the only field-induced magnetic process. This confirms that this process corresponds to a first-order transition.

Determination of the Spontaneous Magnetization. The field dependence of the magnetization along the *b* axis was measured every 5 K. Some curves are shown in Figure 9 (top). At each temperature, the spontaneous magnetization, M_S, can be determined by extrapolating down to zero the $M = f(H)$ data obtained in the field range where the variation is linear, as shown in Figure 9 (top). The temperature dependence of the spontaneous magnetization is represented in Figure 9 (bottom). The spontaneous magnetization vanishes at $T_c = 39$ K. The curve of Figure 9 (bottom) was obtained from the magnetization data along the *b* axis. As expected, strictly the same temperature dependence of the spontaneous magnetization may be deduced from magnetization data measured along the *a* and *c** axes.

(32) Stryjewski, E.; Giordano, N. *Adv. Phys.* **1977**, *26*, 487.
(33) Givord, D.; Li, H. S.; Perrier de la Bathie, R. *Solid State Commun.* **1984**, *51*, 857.
(34) Hirosawa, S.; Matsuura, Y.; Yamamoto, H.; Fujimura, S.; Sagawa, M.; Yamauchi, H. *J. Appl. Phys.* **1986**, *59*, 873.
(35) Salgueiro da Siva, M. A.; Moreira, J. M.; Mendes, J. A.; Amaral, V. S.; Sousa, J. B.; Palmer, S. B. *J. Phys.: Condens. Mater.* **1995**, *7*, 9853.
(36) Canfield, P. C.; Cho, B. K.; Dennis, K. W. *Physica B* **1995**, *215*, 337.
(37) Garcia-Landa, B.; Tomey, E.; Fruchart, D.; Gignoux, D.; Skolozdra, R. *J. Magn. Magn. Mater.* **1996**, *157−158*, 21.
(38) Mendoza, W. A.; Shaheen, S. A. *J. Appl. Phys.* **1996**, 79, 6327.
(39) Cao, G.; McCall, S.; Crow, J. E. *Phys. Rev. B* **1997**, *55*, R672.
(40) Kou, X. C.; Dahlgren, M.; Grössinger, R.; Wiesinger, G. *J. Appl. Phys.* **1997**, *81*, 4428.
(41) Herpin, A. *Théorie du magnétisme*; Presses Universitaires de France: Paris, 1968.

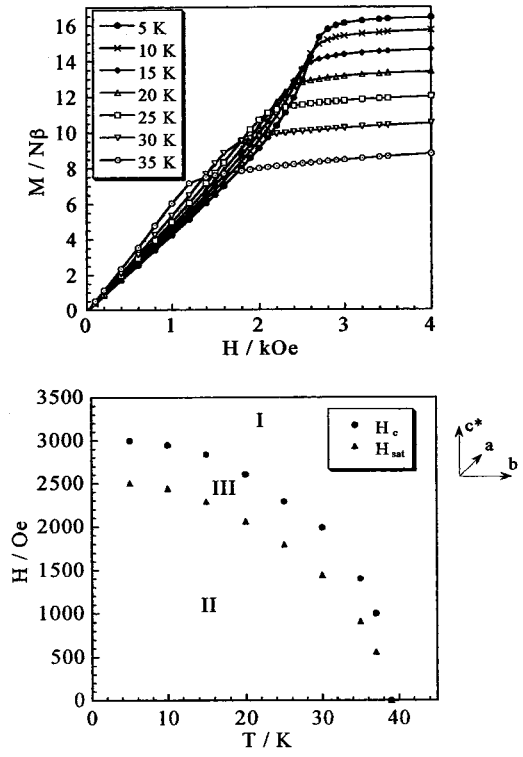

Figure 8. (top) Field dependences of the magnetization measured at different temperatures along the *c** axis. (bottom) Temperature dependence of the critical field, H_c, and of the saturation field, H_{sat}, for a field applied along the *c** direction. The $H_c = f(T)$ and $H_{sat} = f(T)$ curves define three magnetic domains, noted as I−III (see text).

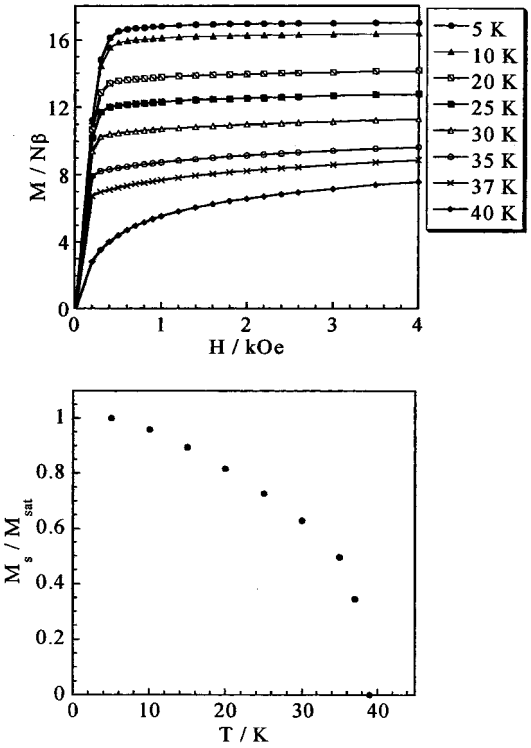

Figure 9. (top) Field dependences of the magnetization along the *b* axis at different temperatures. (bottom) Temperature dependence of the normalized spontaneous magnetization.

Temperature Dependences of the ac Magnetic Susceptibilities. The temperature dependences of the in-phase, χ'_M, and out-of-phase, χ''_M, ac magnetic susceptibilities are represented in Figure 10. Along the three directions, the in-phase responses

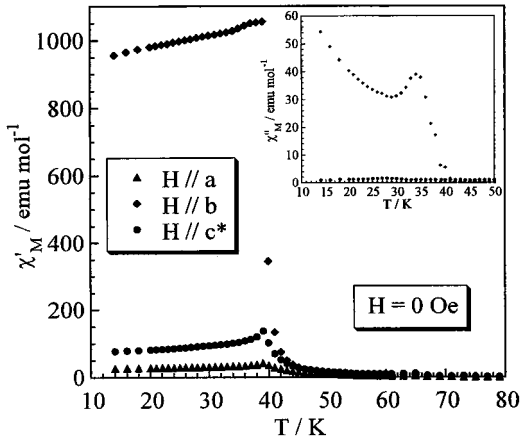

Figure 10. Temperature dependences of the in-phase ac magnetic susceptibility along the *a*, *b*, and *c** axes with a zero static field. In the insert, temperature dependences of the out-of-phase ac magnetic susceptibility along the *a*, *b*, and *c** axes.

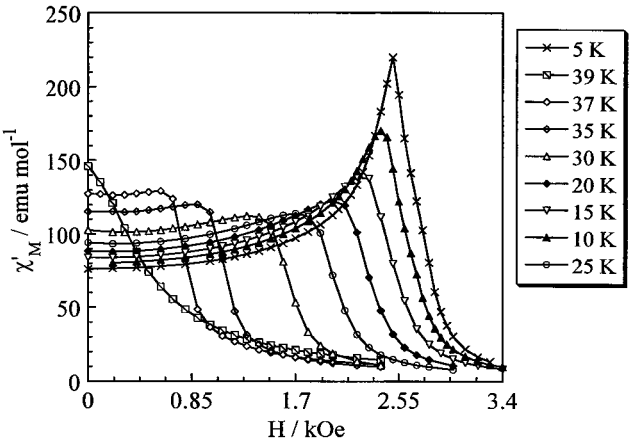

Figure 11. Field dependences of the in-phase ac susceptibilities at different temperatures along the *c** axis.

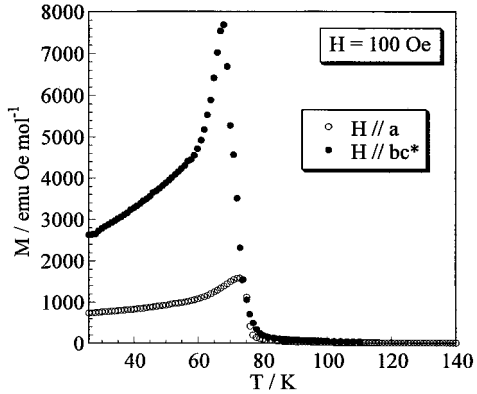

Figure 12. Temperature dependences of the magnetization in the *bc* plane and along the *a* axis under 100 Oe for a partially dehydrated crystal.

exhibit a break around 40 K, the extremes of the derivatives $d\chi'_M/dT$ occurring at $T_c = 39$ K. The χ'_M values along the *b* axis below T_c are much higher than these along the other two directions. The out-of-phase response along the *b* axis is shown in the insert of Figure 12; χ''_M is zero down to 39 K, then presents an abrupt break as *T* is lowered below this temperature, and reaches a maximum around 34 K. Along the other two directions, χ''_M is negligibly weak down to 2 K.

When the field is applied along the easy magnetization axis, *b*, both the displacement of the domain walls and the rotation

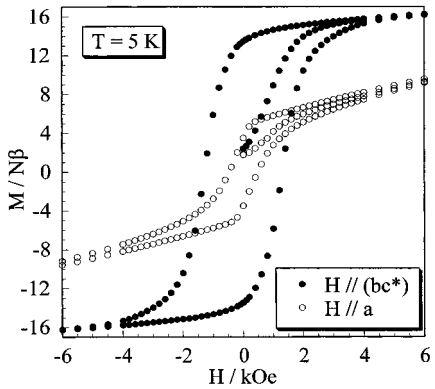

Figure 13. Hysteresis loops in the *bc** plane and along the *a* axis at 10 K for a partially dehydrated crystal.

of the magnetic moments contribute to the ac magnetic response. On the other hand, when the field is applied along a hard magnetization axis, only the rotation of the magnetic moments contributes to the ac response. In the present case, the very high response along *b* as compared to the responses along *a* and *c** indicates that the domain walls move very easily.

Another experiment was performed in the ac mode, namely the field dependence of χ'_M along the *c** axis every 5 K in the magnetically ordered phase. The results are displayed in Figure 11. At each temperature, χ'_M first increases as the field increases, reaches a maximum, then tends to zero at high field. The maximum of χ'_M determines the critical field, H_c, and the extreme of the derivative $d\chi'_M/dH$ determines the saturation field, H_{sat}. The $H_c = f(T)$ and $H_{sat} = f(T)$ curves deduced from this experiment are strictly similar to those shown in Figure 8 (bottom).

Modification of the Magnetic Properties through Partial Dehydration. When a single crystal of $K_2Mn_3(H_2O)_6]Mo(CN)_7]_2 \cdot 6H_2O$ is subjected to a dynamical vacuum with a primary pump for 3 days at room temperature, the noncoordinated water molecules are released. The external shape of the crystal is retained, but its magnetic properties are deeply modified. The $\chi_M T$ versus *T* curve for the partially dehydrated material again reveals ferromagnetic interactions. Above 72 K, the magnetic susceptibility data can be fitted with the Curie−Weiss law $\chi_M = 10.6/(T-72)$.

It was pointed out that the shape of the crystal was not modified through partial dehydration. This suggests that the crystallographic directions are retained, which was confirmed by measuring again the magnetization as a function of the angle between the magnetic field and the crystallographic directions of the nondehydrated material (*ab* and *ac** planes). The temperature dependences of the magnetization were then measured along these directions. The results are represented in Figure 12. The $M = f(T)$ curves along *b* and *c** cannot be distinguished from each other. After dehydration, the *bc** plane may be considered as an easy magnetization plane, even in low field. Both in the *bc** plane and perpendicularly to this plane, the magnetization shows a break at $T_c = 72$ K.

The field dependences of the magnetization were investigated at 10 K both in the *bc** plane and along the *a* direction. The results are displayed in Figure 13. In the easy magnetization plane, the saturation value of 17 Nβ corresponding to the parallel alignment of all the spins is obtained under ca. 5.0 kOe. On the other hand, along the *a* axis, the saturation is not reached yet under 50 kOe. Magnetic hystereses are observed along both directions, with coercive fields of 1.3 kOe in the *bc** plane and 0.55 kOe along *a*. The stabilization of a ferromagnetic state with a strong coercivity through partial dehydration of magnetic molecular materials has already been reported,[42−45] as has the reverse effect of destabilizing a ferromagnetic state.[46]

Discussion

The reaction of $[Mo(CN)_7]^{4-}$ with Mn^{II} ions affords the α- and β-phases of $Mn_2(H_2O)_5Mo(CN)_7 \cdot nH_2O$. Both phases have a three-dimensional structure, and order ferromagnetically at $T_c = 51$ K. The α-phase exhibits an additional magnetic transition, at 43 K in zero field, and the β-phase presents an even more complicated magnetic phase diagram. When the same reaction is carried out in the presence of an excess of K^+ ions, another compound is obtained, to which this paper is devoted. From a structural point of view, this new compound presents many interesting features. It is two-dimensional instead of three-dimensional, the K^+ ions together with noncoordinated water molecules being intercalated between the layers. These layers have a certain thickness; they are made of two parallel gridlike sheets connected to each other by $Mn(CN)_4(H_2O)_2$ units. Moreover, the metal sites are much more distorted than in the α- and β-phases of $Mn_2(H_2O)_5Mo(CN)_7 \cdot nH_2O$. In particular, the coordination polyhedron around Mo^{III} deviates significantly with regard to a regular pentagonal bipyramid; one out of seven cyano groups linked to Mo^{III} is terminal and not bridging, the terminal nitrogen atom of this cyano group interacting with a K^+ ion, and the Mo−C−N−Mn linkages are far from being linear; one of the Mo−C−N bridging angles is equal to 152.1(2)°, and one of the Mn−N−C bridging angles is equal to 143.8(14)°.

As the α- and β-phases of $Mn_2(H_2O)_5Mo(CN)_7 \cdot nH_2O$, the title compound gives very well shaped single crystals, which allowed us to perform a thorough magnetic investigation and to determine the magnetic phase diagram. Despite its two-dimensional character, $K_2Mn_3(H_2O)_6[Mo(CN)_7] \cdot 6H_2O$ orders ferromagnetically, but at a lower temperature than do the α- and β-phases of $Mn_2(H_2O)_5Mo(CN)_7 \cdot nH_2O$, 39 K instead of 51 K. In the magnetically ordered phase, the title compound is very anisotropic. In zero or low field, the easy magnetization axis is *b*. When the field overcomes a certain critical value, the *bc** plane of the layers becomes almost isotropic. The dipolar effects probably play a crucial role in favoring the alignment of the spins in the *bc** plane of the layers. However, the dipolar interactions alone cannot explain the spin reorientation phenomenon occurring in the *bc** plane.

Let us come back to this spin reorientation phenomenon, and to the magnetic phase diagram. The $H_c = f(T)$ and $H_{sat} = f(T)$ curves for a field applied along the *c** axis of Figure 9 (bottom) define three domains, noted as I−III. Domain I corresponds to the paramagnetic domain in which the spins are either randomly oriented or aligned along the field direction. Domain II corresponds to the ferromagnetically ordered domain in which the spins are aligned along the *b* axis. Domain III, finally, is a mixed domain in which the spins rotate from the *b* to the *c** direction as the field increases from H_c to H_{sat}. The frontier between the domains I and III corresponds to a second-order phase transition, and that between the domains II and III

(42) Nakatani, K.; Bergerat, P.; Codjovi, E.; Mathonière, C.; Pei, Y.; Kahn, O. *Inorg. Chem.* **1991**, *30*, 3977.
(43) Turner, S.; Kahn, O.; Rabardel, L. *J. Am. Chem. Soc.* **1996**, *118*, 8, 6428.
(44) Larionova, J.; Chavan, S. A.; Yakhmi, J. V.; Gulbrandsen Froystein, A.; Sletten, J.; Sourisseau, C.; Kahn, O. *Inorg. Chem.* **1997**, *36*, 6374.
(45) Re, N.; Crescenzi, R.; Floriani, C.; Miyasaka, H.; Matsumoto, N. *Inorg. Chem.* **1998**, *37*, 2717.
(46) Van Langenberg, K.; Batten, S. R.; Berry, K. J.; Hockless, D. C. R. Moubaraki, B.; Murray, K. S. *Inorg. Chem.* **1997**, *36*, 5006.

corresponds to a first-order phase transition. The microscopic origin of the spin reorientation is not totally clear to us. This phenomenon might result from a competition between dipolar interactions and shape anisotropy. What deserves to be pointed out is that a partial dehydration of the compound apparently does not modify the orientation of the crystallographic axes, but suppresses the spin reorientation. For the partially dehydrated material, the *bc** plane of the layers is an easy magnetization plane under any field.

The partial dehydration not only suppresses the spin reorientation, but also shifts T_c up to 72 K and increases the hardness of the ferromagnet. The upward shift of T_c may be attributed to the fact that the release of noncoordinated water molecules situated in the gap between the layers makes these layers closer to each other. The coercivity in the partially dehydrated material is probably due to the structural defects created by the release of water molecules. It would be quite interesting to obtain structural information on the partially dehydrated phase. Such a study is underway.

In this work, the measured magnetizations were not corrected for the demagnetizing field effects. We would like to emphasize that such corrections would not modify our conclusions. As a matter of fact, the interesting physics occurs in the *bc** plane of the layers, and owing to the shape of the crystals (see Figure 4), the corrections of demagnetizing field effects along *b* and *c** should be very similar.

An important aspect of this work concerns the ferromagnetic nature of the interaction between Mo^{III} and Mn^{II} ions through the cyano bridge. This problem has been extensively discussed in our previous paper to which the reader may refer.

Conclusion

A new family of cyano-bridged bimetallic compounds has been discovered whose richness in terms of both structures and physical properties is exceptional. The compounds of this family possess a remarkable capability to grow as well-shaped single crystals, and the physical studies performed on these single crystals reveal many peculiarities. Not only are the compounds reported so far ferromagnets, but they exhibit many interesting features in addition to the ferromagnetic ordering, such as the presence of several magnetically ordered phases (for the α- and β-phases of $Mn_2(H_2O)_5Mo(CN)_7 \cdot nH_2O$) and spin reorientations. To the best of our knowledge, these features have not been investigated so far in the field of molecular magnetism. A key role in this interesting physics is played by the extremely strong anisotropy of the compounds. This anisotropy has two origins, namely the structural anisotropy and the local anisotropy of the low-spin Mo^{III} ion.

We intend to explore further the chemistry and physics of the compounds of this family, and hope to be able to report soon on new compounds with even more elaborated supramolecular architectures.

Acknowledgment. This work was partly funded by the TMR Research Network ERB 4061 PL-97-0197 of the European Union, entitled "Molecular Magnetism: From Materials toward Devices."

Supporting Information Available: Listing of crystal data and structure refinement, atomic coordinates, bond lengths and angles, anisotropic displacement parameters (PDF). This material is available free of charge via the Internet at http://pubs.acs.org.

JA9832717